Science of the Total Environment 779 (2021) 146283

Contents lists available at ScienceDirect

Science of the Total Environment

journal homepage: www.elsevier.com/locate/scitotenv

Underestimated or overestimated? Dynamic assessment of hourly $PM_{2.5}$ exposure in the metropolitan area based on heatmap and micro-air monitoring stations

Xin Li [a,1], Tao Yang [b,1], Zhuotong Zeng [c,1], Xiaodong Li [a,1], Guangming Zeng [a,*], Jie Liang [a,*], Rong Xiao [c,*], Xuwu Chen [a]

[a] College of Environmental Science and Engineering, Hunan University, Changsha 410082, PR China
[b] School of Architecture, Hunan University, Changsha 410082, PR China
[c] Department of Dermatology, Second Xiangya Hospital, Central South University, Changsha 410011, PR China

HIGHLIGHTS

- The LBS big data of Heatmap is suitable for depicting the short-term population mobility;
- The downtown' PWE is often overestimated, while the underrated PWE is mainly in suburbs, especially on weekends;
- The urban PWE to high-level $PM_{2.5}$ is greatly underestimated during the morning rush hours on weekdays;
- The commuters may suffer more $PM_{2.5}$ pollution and uneven environmental resource distribution

GRAPHICAL ABSTRACT

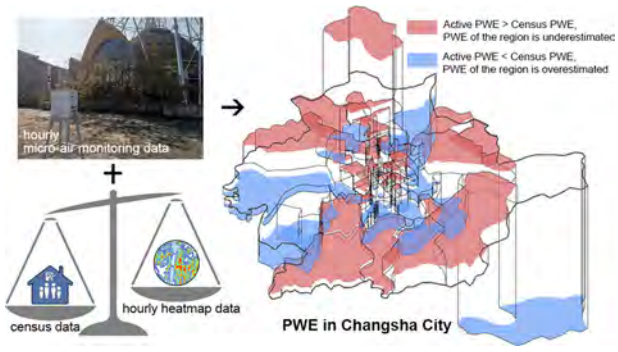

ARTICLE INFO

Article history:
Received 15 December 2020
Received in revised form 22 February 2021
Accepted 1 March 2021
Available online 8 March 2021

Editor: Pavlos Kassomenos

Keywords:
Short-term population mobility
Big data
Suburbanization
Short-term $PM_{2.5}$ exposure assessment, metropolitan area

ABSTRACT

Spatio-temporal distributions of air pollution and population are two important factors influencing the patterns of mortality and diseases. Past studies have quantified the adverse effects of long-term exposure to air pollution. However, the dynamic changes of air pollution levels and population mobility within a day are rarely taken into consideration, especially in metropolitan areas. In this study, we use the high-resolution $PM_{2.5}$ data from the micro-air monitoring stations, and hourly population mobility simulated by the heatmap based on Location Based Service (LBS) big data to evaluate the hourly active $PM_{2.5}$ exposure in a typical Chinese metropolis. The dynamic "active population exposure" is compared spatiotemporally with the static "census population exposure" based on census data. The results show that over 12 h on both study periods, 45.83% of suburbs' population-weighted exposure (PWE) is underestimated, while 100% of rural PWE and more than 34.78% of downtown's PWE are overestimated, with the relative difference reaching from −11 μg/m^3 to 7 μg/m^3. More notably, the total PWE of the active population at morning peak hours on weekdays is worse than previously realized, about 12.41% of people are exposed to $PM_{2.5}$ over 60 μg/m^3, about twice as much as that in census scenario. The commuters who live in the suburbs and work in downtown may suffer more from $PM_{2.5}$ exposure and uneven environmental resource distribution. This study proposes a new approach of calculating population exposure which can also be extended to quantify other environmental issues and related health burdens.

* Corresponding authors.
E-mail addresses: dklixin@hnu.edu.cn (X. Li), yangt@hnu.edu.cn (T. Yang), zengzhuotong@csu.edu.cn (Z. Zeng), lxdfox@hnu.edu.cn (X. Li), zgming@hnu.edu.cn (G. Zeng), liangjie@hnu.edu.cn (J. Liang), xiaorong65@csu.edu.cn (R. Xiao), cxw6868@hnu.edu.cn (X. Chen).
[1] Co-first author.

https://doi.org/10.1016/j.scitotenv.2021.146283
0048-9697/

1. Introduction

Air pollution, especially particulate matter of aerodynamic diameter ≤2.5 μm ($PM_{2.5}$) has become a major public health concern in recent years (Cohen et al., 2017; Kampa and Castanas, 2008; Kim et al., 2015). Many studies have found both acute (Dominici et al., 2006; Laden et al., 2000; Peters et al., 2001) and chronic (Hoek et al., 2013; Miller et al., 2007) exposure to high-level $PM_{2.5}$ can result in premature deaths associated with various health conditions, such as cardiovascular, respiratory and reproductive system diseases. It is particularly worrying that $PM_{2.5}$ pollution is more serious in China (Apte et al., 2015; Lin et al., 2018). Especially in the high-density metropolitan areas, $PM_{2.5}$ concentrations can be greater than 200 μg/m^3 during heavy hazy days (Chan and Yao, 2008; Li et al., 2017; Liu et al., 2013). According to Asian Development Bank, in 2013, less than 1% of 500 biggest cities in China (with population of more than 100,000) met the standard of World Health Organization (WHO) Air Quality (annual mean value: 10 μg/m^3, 24-h mean value: 25 μg/m^3) (Zhang and Crooks, 2012). In addition, the population mobility with Chinese characteristics such as excessive commutes may lead urban people to suffer more $PM_{2.5}$ exposure and unfair environmental resource distribution (Day and Cervero, 2010; Lu et al., 2017). Thus, precisely assessing short- and long-term population exposure to $PM_{2.5}$ in Chinese metropolises become crucial for better understanding the risk and taking valid interventions.

Over the past years, researchers have investigated several standards for the evaluation of population exposure risks of $PM_{2.5}$. They confirm the big differences of personal exposure in various spatio-temporal scenarios (Nethery et al., 2008). Different micro-environments (spatial heterogeneity of $PM_{2.5}$) and human activities are major determining factors of population exposures, thus, both of them should be taken into account. However, it is difficult to estimate population exposure to $PM_{2.5}$ in high resolution of both time and space in the whole metropolitan area. For depicting map of ground $PM_{2.5}$ distribution, site-based observations and satellite-based models are most widely used to get relatively reliable $PM_{2.5}$ data. Site-based observations offer the real-time estimations of $PM_{2.5}$ concentration levels through continuous point-based interpolating measurements provided by monitoring stations (Li et al., 2015; Liu et al., 2015; Xu et al., 2019; Zhang et al., 2016). But the sparse and uneven distribution of stations cannot fully capture the spatial variability, which may limit accuracy of the interpolation results. The satellite-based models help improve the spatial precision of $PM_{2.5}$ concentrations. Scholars combine values of aerosol optical depth (AOD) with various models (e.g. global atmospheric chemistry model (Gariazzo et al., 2020), land use regression model (Nyhan et al., 2019) and random-forest model (Araki et al., 2018; Stafoggia et al., 2019)) to map ground $PM_{2.5}$ concentrations. Nevertheless, the satellite data is sensitive to weather, and scholars prefer to consider a relatively big temporal resolution of daily, monthly or yearly of change of $PM_{2.5}$.

Accurately estimating the dynamic population activity is another challenging point in the assessment of population exposure. Census data is easily available and usually applies to country-scale models over decades as it assumes that the population distribution is uniform and it is only updated every five or ten years (Fleischer et al., 2014; Zhao et al., 2018). The raster datasets, such as LandScan Global Population (Dobson et al., 2000) and WorldPop (Tatem et al., 2005) show some spatial heterogeneity of population. However, like census, they also ignore the constant flow of population. Previous studies have shown the health risks may be underestimated when population mobility is not considered in the exposure assessment (Setton et al., 2011). To solve the problem, scholars take the people's location information into amount. Some use GPS-based mobile air monitors to examine subjects' real-time location and the air pollution concentration nearby (Hankey et al., 2019; Lu and Fang, 2015). However, due to the individual differences, privacy restrictions and spatial misalignment from the spatial aggregation of mobile measurements, this method is hard to be applied in a wide area. Some studies develop mobile signal data to simulate spatial patterns of human activity and to assess the long-term exposure to $PM_{2.5}$ (Chen et al., 2018; Nyhan et al., 2016). This method greatly improves the precision of both time and space, but the source data of population is hard or costly to obtain. In addition, it should be noted that the short-term exposure such as hourly exposure to air pollution gets less attention. Actually, $PM_{2.5}$ can change dramatically across temporal scales from minutes to hours in big cities, and most people cannot stay still in areas of the same air quality throughout the whole day. Short-term exposure is a good indicator to assess the impact of $PM_{2.5}$ on urban people, especially certain groups like commuters.

To quantify the real-time population exposure in metropolises, this study integrates the air pollution data from densely distributed micro-air monitoring stations in Changsha City (including the central urban areas, rural areas and suburbs) and dynamic population distribution information from LBS big data of the heatmap. Then we compare the short-term (per hour) exposure of urban people in two population distribution computing models and pay special attention to the people's exposure in rush hours. The purpose of our study is to improve the methods of quantifying short-term assess population exposure to air pollution in large cities, to locate high exposure areas more accurately, and to provide a new idea for future research in environmental epidemiology and urban planning.

2. Materials and methods

2.1. Study area

We investigated the hourly concentrations of $PM_{2.5}$ in Changsha City from April 1st to April 28th in 2019 (see the April's hourly $PM_{2.5}$ data in Table S2 which shows similar time trend every week), and selected five typical days (April 19th to April 23rd), including three working days and two rest days. Then we assessed the hourly (7:00 am to 11:00 pm) PWE to $PM_{2.5}$ during the five days. Changsha is a typical Chinese metropolis with characteristics of high density and centralized urban function. Xiang River divides this city into two parts, the east is downtown while the west is mainly suburbs and scenic spots. The special city configuration and structure lead to vast population who live in the west and work in the east commuting across the city every day. The study area (see Fig. S1) is Changsha main city which occupies 1837 km^2, including 73 street-level communities (including 46 central regions, 24 suburban regions and 3 rural regions, mainly divided by Changsha belt high way) with 3.27 million of residents.

2.2. Fine particulate matter data

The $PM_{2.5}$ concentration data was obtained from the micro-air monitoring stations. By the end of 2018, 162 micro-air monitoring stations were set up by government in Changsha, including 122 in the main urban areas (as shown in Fig. 1), at least one or two in each street-level community which is the smallest administrative unit consistent with the census unit (the distance between the stations is about 500 m in downtown areas, and 2 km in the suburbs). This plan makes up for the lack of the number of state controlling air sampling sites and aims to provide Changsha City with accurate monitoring data, so when the air pollution rising over an acceptable level, the managers can quickly determine the location and conduct inspections in time. The micro-air monitoring stations adopt the particle sensor with laser scattering to monitor normal pollutants of $PM_{2.5}$ and PM_{10}. Like the state controlling air sampling sites' data, the monitoring data of micro-air monitoring stations is also regulated by Ecology and Environment Department of Hunan to meet the same national standards. The air pollutant data is uploaded every hour through the network and can be seen on the environmental quality monitoring platform in real time. The original air pollution data we got from the micro-air monitoring stations is in high spatio-temporal precision. (See detailed description of the accuracy of air pollution data in Method S1).

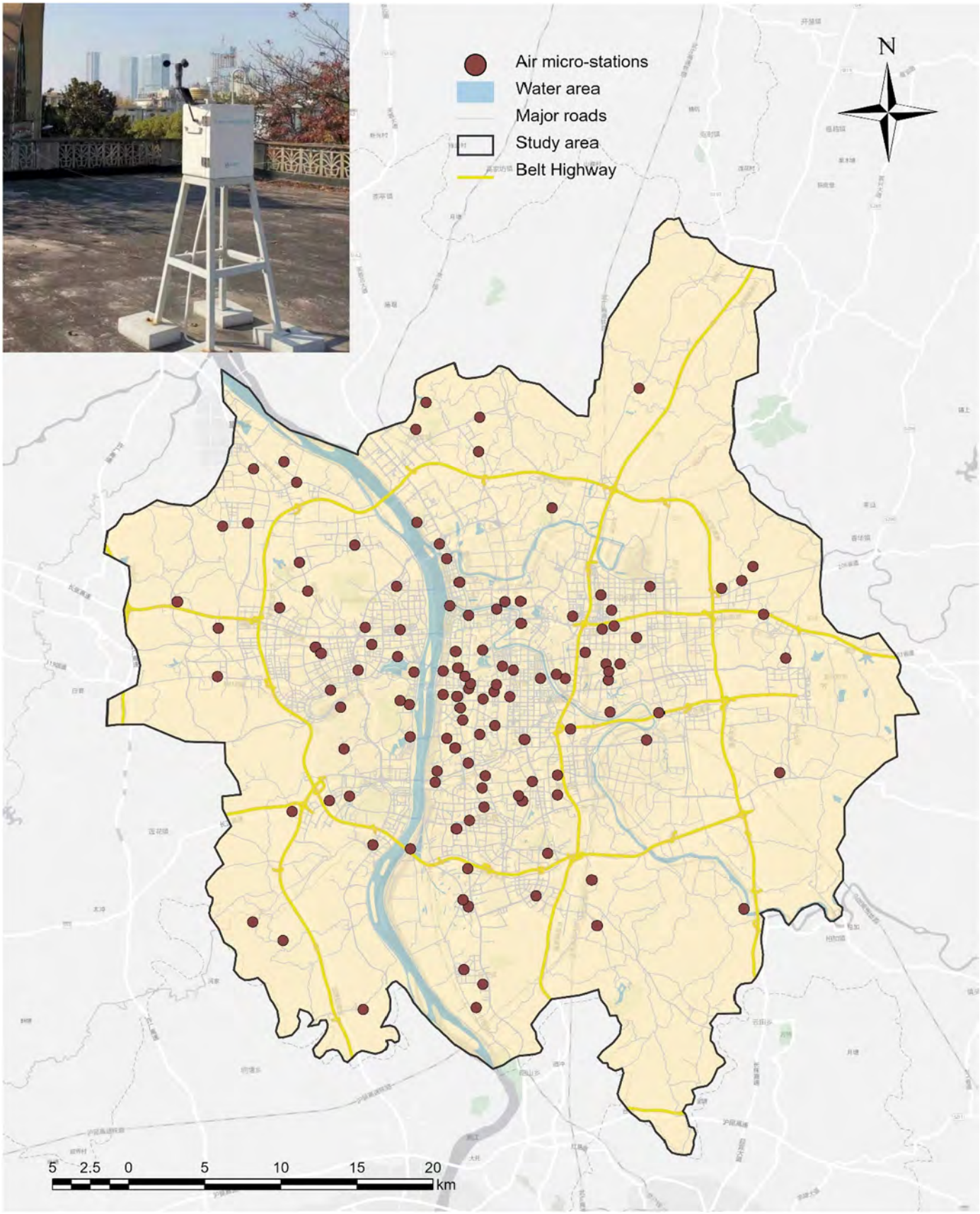

Fig. 1. Locations of micro-air monitoring stations in Changsha main city.

The $PM_{2.5}$ spatial distribution map was realized by the Cokriging spatial interpolation method, which used PM_{10} data as auxiliary information. The Cokriging is based on Kriging spatial interpolation with higher accuracy and has been effectively used to map the spatial distribution pattern of air pollution (Carnevale et al., 2011; Singh et al., 2011; Wu et al., 2006). The $PM_{2.5}$ and PM_{10} measured values from April 19th to April 23rd were processed by Cokriging interpolation to generate grid-layer graphs with a resolution of 100 m × 100 m. Then we took the average of all pixels in each street community per hour, and finally got the hourly street-level $PM_{2.5}$ concentrations separately on weekdays and weekends.

2.3. Quantifying dynamic population distribution based on heatmap

Geographic and time-referenced heatmap data was used to quantify the hourly number of populations in each district throughout the study period. Heatmap is a big-data visual product launched by Baidu (one of the largest Internet firms in China), when the smartphone users access Baidu products (such as search, map, weather, music, etc.), the clusters location information is uploaded to the platform. As Baidu heatmap is based on LBS platform, we define the data as LBS big data of the heatmap in the research. According the official introduction of the heatmap, the accuracy of positioning of Baidu App is about 1–3 m. The "Heat Index" is obtained by counting the speed and density of people, with different color and brightness reflecting the spatial difference of population size. The data is updated about every 15 min. As a new application based on hundreds of millions user's location information, LBS big data of the heatmap can cover enough of the smart phone users (see detailed description of the accuracy of LBS data in Method S2). According to "The 44th China Statistical Report on Internet Development" (China Internet Network Information Center, 2019) published by China Internet Network Information Center, up to June 2019, there were 854 million Internet users and 847 million mobile phone users in China. Among the mobile users, urban population accounted for 73.71%. With a big sample size and full-covered population composition, the population calculated by LBS big data of the heatmap can meet the demand of this research.

The difference of human activity in cities mainly reflects on the regular activities such as commute and free movement like leisure. Thus, we selected the heatmaps updated every hour from 7 am to 11 pm in five days from April 19th to April 23rd, then averaged and classified the data into weekday group and weekend group, finally got 34 pieces of heatmaps. The study made coordinate conversion parameters through Baidu API application programming interface, and transferred the images in the database to the geographic coordinate system of this article under the ArcGIS Pro platform. There were four terminals of the heatmap images, normally the fourth terminal was extracted, as this Alpha terminal can expressed the information of maps by 256 levels of gray, easy for reclassify and reassignment (Tai, 2019; Wang, 2018; Wu and Ye, 2016). Finally, the population distribution data was quantified by identifying the pixel level and scale in each administrative region.

2.3.1. Statistics of active population

The total active population of a region was the sum of each pixel's population in the region, which was characterized by the sum of the product of the pixel size and its people density. Specifically, the equation is listed as follows:

$$P_{ik} = \delta \times d_{ik} \tag{1}$$

$$P_n = \sum_{i=1}^{h} P_{ik} \times j_k \tag{2}$$

where n represents different street-level communities (regions); i represents the serial number of spatial unit (pixel unit); k represents the color number of heatmap; P_{ik} is the active population of the k-th color value at spatial unit i; δ is the area of a pixel unit in the region (the area of the pixel in this study is 100 square meters); d_{ik} is the active population density of the k-th color value at spatial unit i. The estimation of population density refers to the Baidu official legend; the color value and brightness jointly represent the population density (Leng et al., 2015; Tan et al., 2016). P_n is the total active population in the region n; h is the total number of color value categories; and j_k represents the number of pixels of the k-th color value in n-th region.

As users have the dynamic characteristics of constantly "online" and "offline", the total number of active populations at different moments may fluctuate. In order to avoid interference from changing sample size due to the different habit of using mobile phone, the distribution of active population was expressed by proportion of active population as follows:

$$PP_{mi} = \frac{P_{mi}}{P_{mn}} \tag{3}$$

$$PP_{mn} = \frac{P_{mn}}{\sum_n P_{mn}} \tag{4}$$

where m represents different times, PP_{mi} represents the proportion of the population at spatial unit i at time m, P_{mi} represents the number of active population at spatial unit i at time m, P_{mn} is the number of active population in the n-th region at time m, and PP_{mn} is the proportion of the active population in the n-th region to the total active population in all regions at time m.

2.4. Census population

The Changsha City demographic data in 2019 was obtained from WorldPop Country Datasets (Hay et al., 2005; Tatem et al., 2005, 2004; Tatem and Hay, 2004) (https://www.worldpop.org/). As described in the Introduction part, population and housing census is still the most important resource for producing accurate population data at national and subnational scales. WorldPop top-down modelling methods take a global database of administrative unit-based census and projection counts for each year of nearly 20 years and adopt a set of detailed geospatial datasets to break them into grid cell-based counts. WorldPop has developed peer-reviewed spatial statistical methods, using Random Forests machine learning methods to transform and disaggregate population counts at administrative unit levels to 100 × 100 m grid, utilizing relationships with spatial covariate layers from satellites and other sources (Reed et al., 2018; Stevens et al., 2020, 2015). We adopt a grid map of the WorldPop population distribution of Changsha City in 2019. The total urban population of Changsha City according to WorldPop figures was 3.27 million in 2019. After a summary calculation, the percentage of population in each street-level administrative unit of the total urban population was obtained as the "census population" in this paper.

2.5. Population-weighted exposure to $PM_{2.5}$

We adopted PWE assessment which can take the spatial distribution of population into account as well as compare the exposure risk of different regions (Gui et al., 2019; Li et al., 2019). For accurately superimposing different types of layers in following steps, the study used a unifying temporary and spatial resolution of the $PM_{2.5}$ concentration distribution and heatmap data, as 1 h and a grid of 100 m × 100 m, respectively. This pixel-based method for assessing PWE can efficiently avoid the potential zoning effect of the modifiable area unit problem (MAUP) (Chan et al., 2012; Ho et al., 2015). The Eq. (5) below was used to estimate PWE to $PM_{2.5}$ in different regions of Changsha City for later comparison.

$$E_{mn} = \frac{\sum_{i=1}^{j} (P_{mi} \times PM_{mi})}{P_{mn}} \tag{5}$$

where E_{mn} is the PWE to $PM_{2.5}$ in the n-th region of Changsha City at time m, P_{mi} represents the number of active population at spatial unit i at time m, P_{mn} is the number of active population in the n-th region at time m, PM_{mi} is the $PM_{2.5}$ concentration at spatial unit i at time m, and j is the total number of units in region n.

3. Results

3.1. Spatio-temporal variation of $PM_{2.5}$ and population mobility

3.1.1. Spatio-temporal patterns of $PM_{2.5}$ in Changsha

Fig. 2 illustrates the hourly $PM_{2.5}$ concentrations in Changsha during the study periods (the $PM_{2.5}$ data in 5 days was averaged and classified into weekday group and weekend group). In general, the $PM_{2.5}$ pollution is more serious and shows a more obvious spatial heterogeneity on weekends, which may be because of the large numbers of construction projects in Changsha, and the busy nights' and weekends' operation on building sites. Specifically, the average concentration on weekends is higher than that on weekdays by 15.03%, and the difference between the highest and the lowest values exceed over 60 μg/m^3 on weekends, which is twice the difference on workdays. The temporal trend of $PM_{2.5}$ concentration on both days is similar, but the spatial pattern varies greatly. For example, the peak appears on morning rush hours, with mean values of 53 μg/m^3 on weekdays and 66 μg/m^3 on weekends, respectively. Then the $PM_{2.5}$ concentrations decrease slowly to the low of 40 μg/m^3 on weekdays and 50 μg/m^3 on weekends in evening rush hours and rises again at night on both days. However, in terms of the spatial distribution, the hot spots are concentrated in the west of Changsha City (new development zones) on weekdays. While on weekends, areas of high $PM_{2.5}$ concentration expand to downtown, western industrial and eastern airport regions. (Detailed distribution map of $PM_{2.5}$ concentration during different periods are shown in Fig. S2.)

3.1.2. Trend of population mobility based on LBS big data of the heatmap

Fig. 3a and b shows the average proportion of active population in different regions calculated by heatmap in Changsha City at 10 am (working time) and 10 pm (rest time) on weekdays, collectively referred to as the "active population" in the study. Fig. 3c is the relative difference between the proportion of active population at upper two time points, expressing the trend of population mobility. Overall, the crowds are spreading from the city center to the suburbs from daytime to night. Among them, Zuojiatang Street (District 53 in downtown) has the largest number of people leaving at night, losing 1.1% of population. While Xingsha Street (District 61 in suburb) is the area with the most people streaming into at night, a 1.9% increase over morning. These findings are consistent with the actual condition. Fig. 3d displays the proportion of census population, in relative terms, is evenly distributed, which shows a significant difference in comparison with the proportion of the active population.

3.2. Relative differences between dynamic and static exposure

3.2.1. Hourly spatio-temporal patterns of active PWE and census PWE

In the study, hourly PWE of all regions in the main urban area of Changsha is calculated in the scenario of "active population" and "census population". We choose 8:00, 10:00, 18:00, and 22:00 as typical

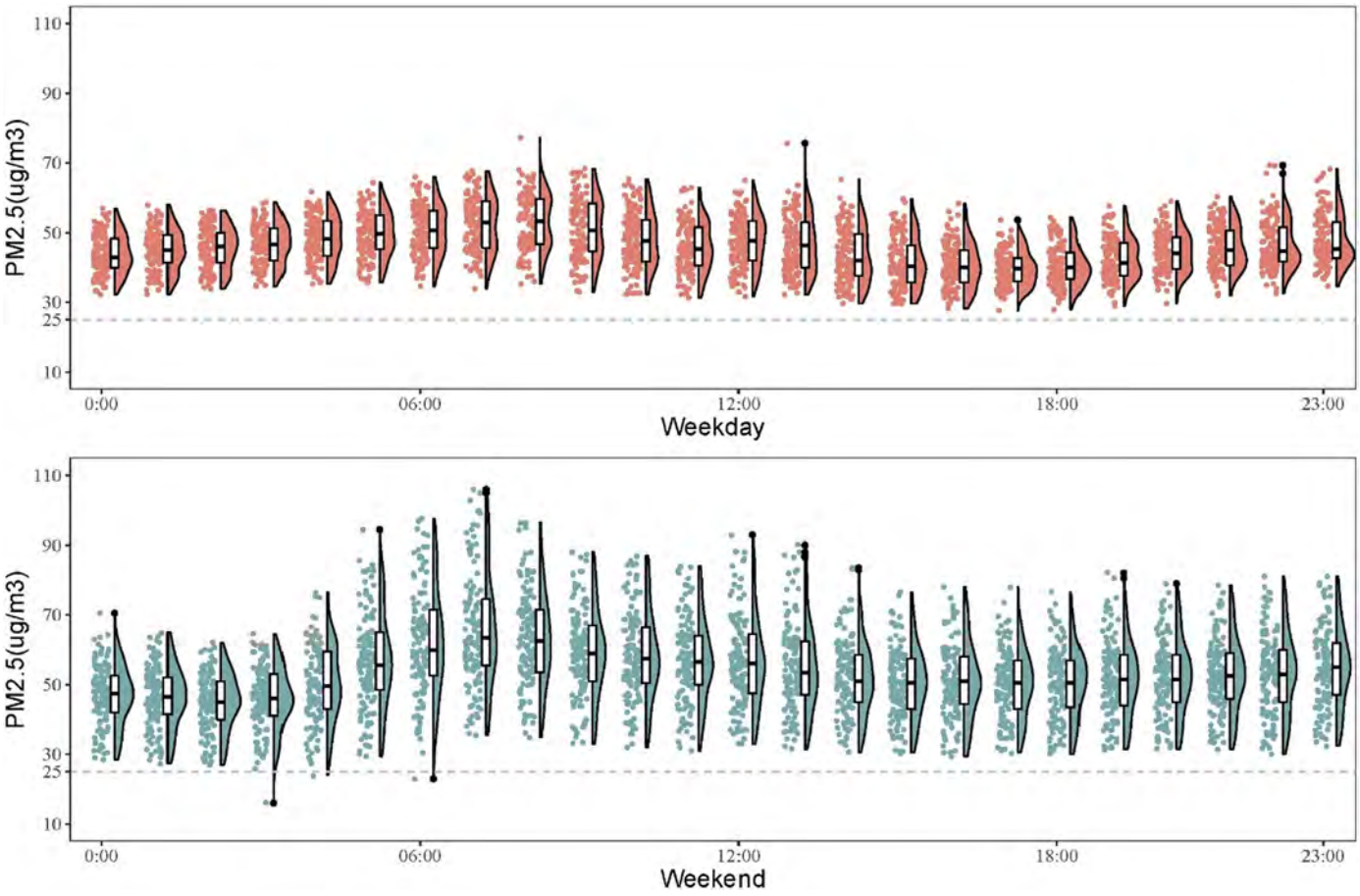

Fig. 2. Scatter-box plots of hourly $PM_{2.5}$ concentration levels in Changsha main city during the study periods (the $PM_{2.5}$ data in 5 days was averaged and classified into weekday group and weekend group, and each point represents $PM_{2.5}$ concentration in corresponding region).

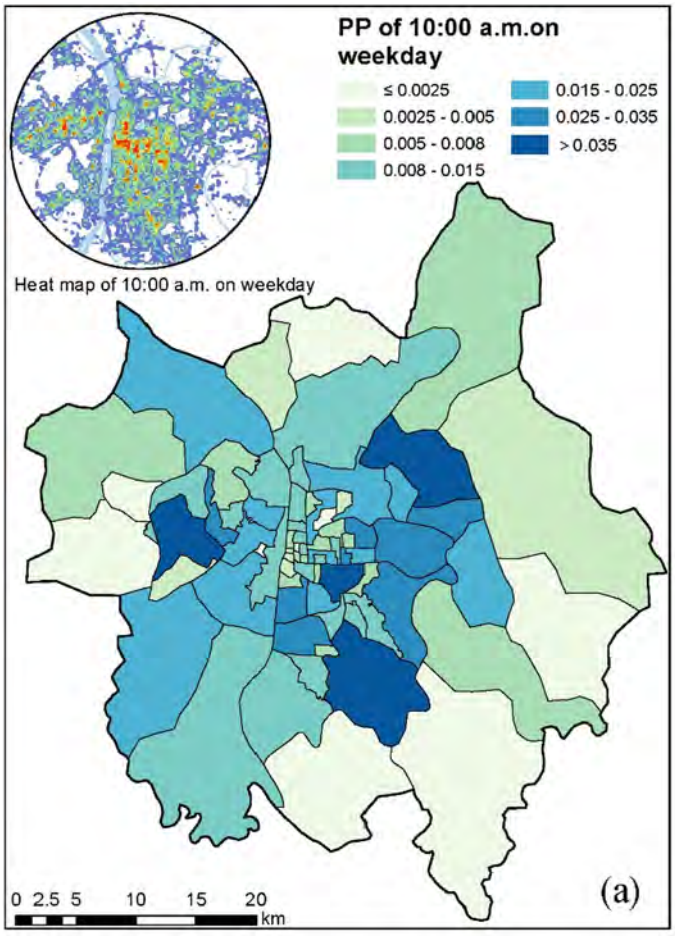
PP of 10:00 a.m.on weekday
≤ 0.0025
0.0025 - 0.005
0.005 - 0.008
0.008 - 0.015
0.015 - 0.025
0.025 - 0.035
> 0.035
Heat map of 10:00 a.m. on weekday
0 2.5 5 10 15 20
km
(a)

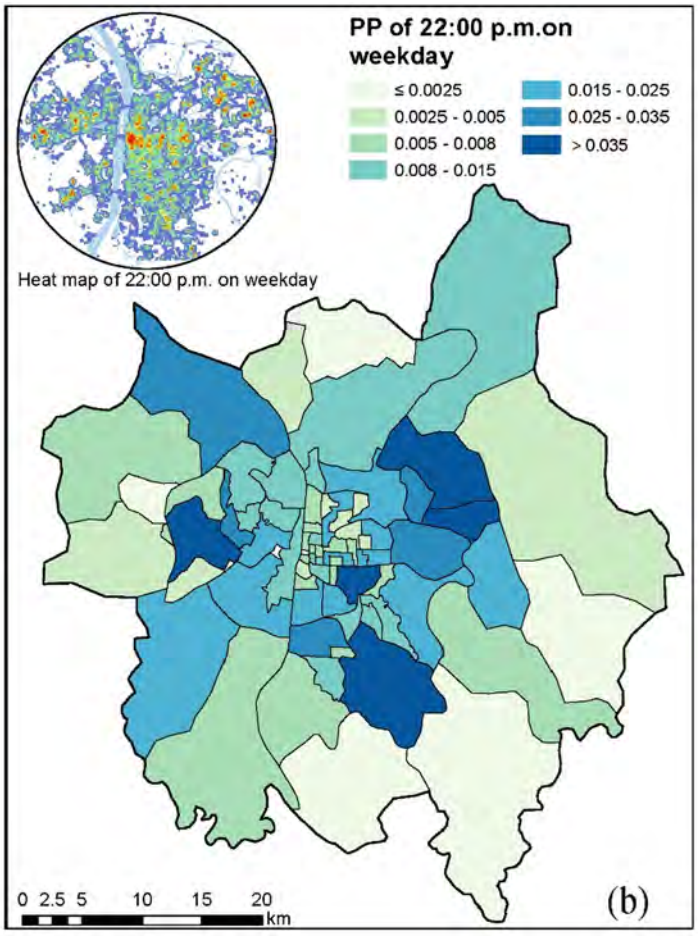
PP of 22:00 p.m.on weekday
≤ 0.0025
0.0025 - 0.005
0.005 - 0.008
0.008 - 0.015
0.015 - 0.025
0.025 - 0.035
> 0.035
Heat map of 22:00 p.m. on weekday
0 2.5 5 10 15 20
km
(b)

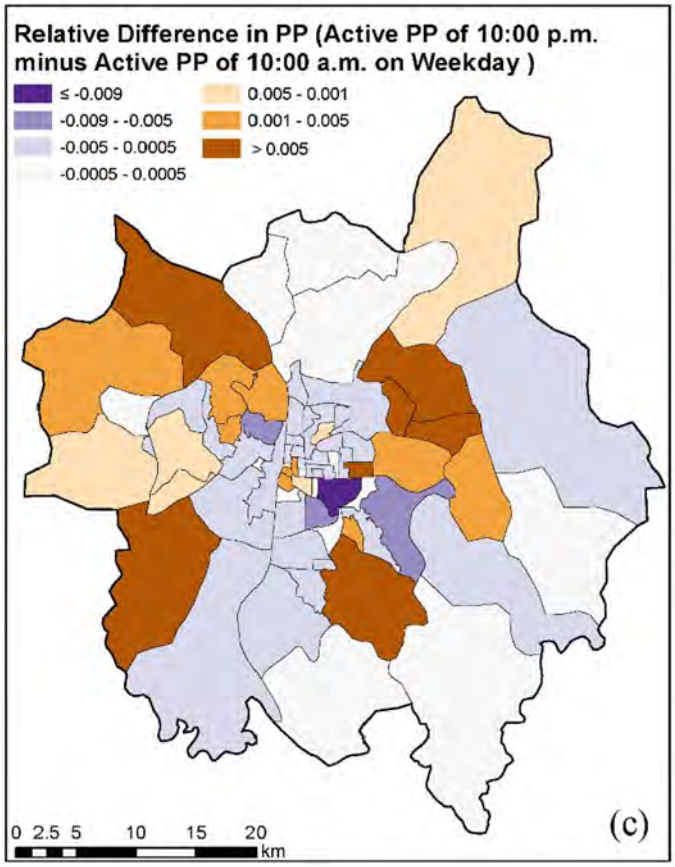
Relative Difference in PP (Active PP of 10:00 p.m. minus Active PP of 10:00 a.m. on Weekday)
≤ -0.009
-0.009 - -0.005
-0.005 - 0.0005
-0.0005 - 0.0005
0.005 - 0.001
0.001 - 0.005
> 0.005
0 2.5 5 10 15 20
km
(c)

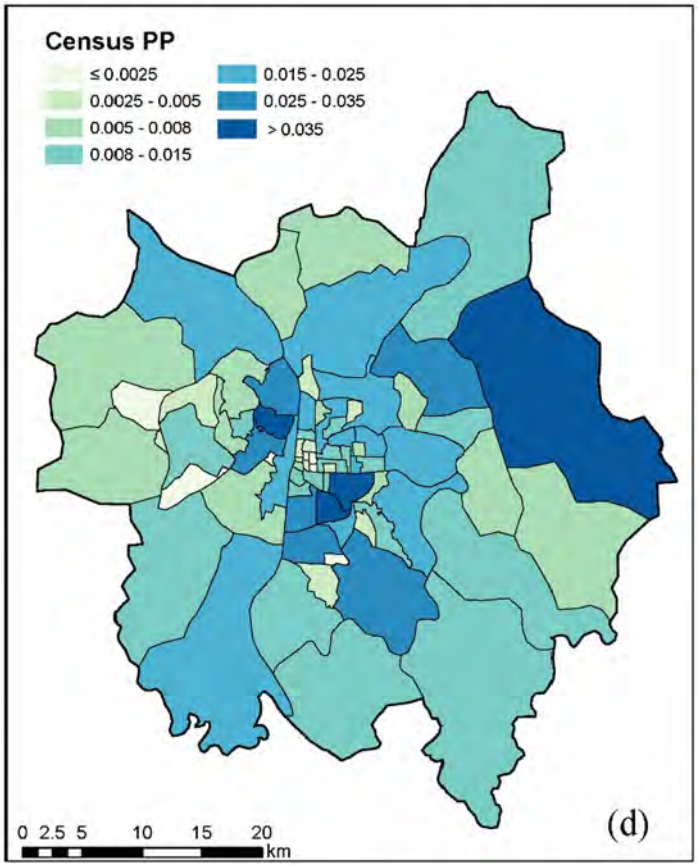
Census PP
≤ 0.0025
0.0025 - 0.005
0.005 - 0.008
0.008 - 0.015
0.015 - 0.025
0.025 - 0.035
> 0.035
0 2.5 5 10 15 20
km
(d)

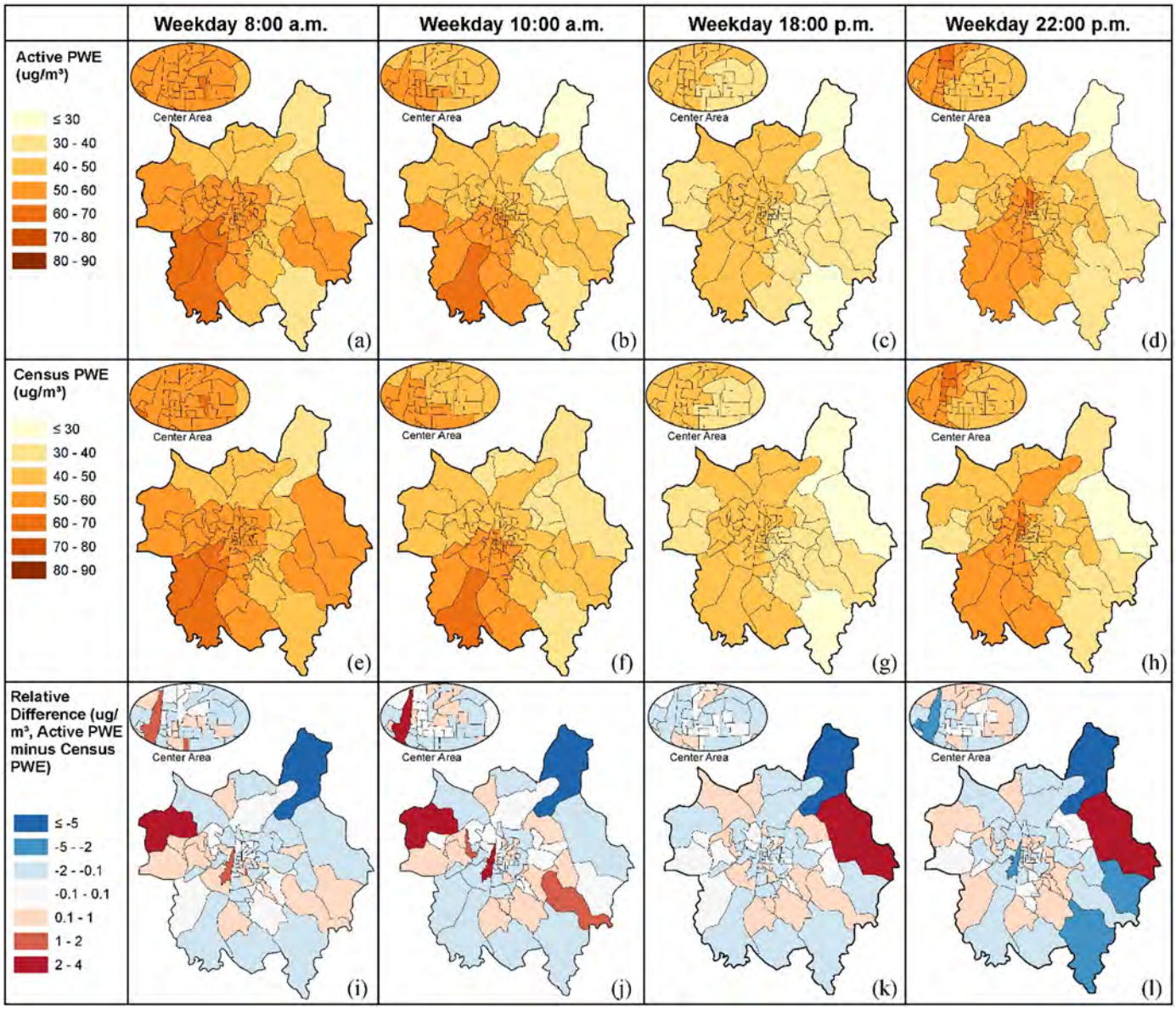

Fig. 4. (a)–(d) Map of hourly PWE to $PM_{2.5}$ ($\mu g/m^3$) per district for the active population scenario on weekdays, (e)–(h) for the census population scenario on weekdays. (i)–(l) The relative difference ($\mu g/m^3$) between these two scenarios on weekdays. (Blue indicates PWE of the region is overestimated, while red indicates the PWE is underestimatEd.) (For interpretation of the references to color in this figure legend, the reader is referred to the web version of this article.)

times from 17 time points on both weekdays and weekends. Figs. 4 and S3 describe the changes in PWE to $PM_{2.5}$ during the eight time periods selected. The overall temporal trend of the population-weighted $PM_{2.5}$ exposure generated in the two scenarios is consistent with the actual $PM_{2.5}$ concentration, all reaching the highest peak in morning rush hours, falling slowly during the day, and increasing slightly again at night.

There are some differences of actual spatial PWE distribution in the two scenarios, with certain rules. As can be seen in Fig. 4a–h, areas of high exposure value are dispersedly distributed among suburban central areas in west and central business areas on weekdays. While on weekends, the high-value areas are more concentrated in the city center and transport hub zones in east. Among them, the hot spots such as No. 1 Wenyi Road Street, No. 8 Wulipai Street, No. 12 Xianghu Street and No. 9 Huoxing Street which are all typical downtown areas ranked steadily within top 5 in all 17 h monitored throughout the two days. The distribution of hot spots are similar with the previous research, indicating that the downtown exposure to $PM_{2.5}$ is very serious (Lee et al., 2017; Li et al., 2013; Rijnders et al., 2001; Xu et al., 2019; Zhang et al., 2016). The Table S1 records the areas of top 5 highest $PM_{2.5}$ exposure in detail.

3.2.2. Comparison of hourly active PWE and census PWE

The relative difference is calculated to compare the dynamic exposure with the static exposure. We define the exposure is underestimated or overestimated of the regions where the active PWE is higher or lower than the census PWE. From Figs. 4i–l, S3i–l, we can see the suburbs' PWE is largely underestimated especially on weekends, while the overestimated PWE is mainly in rural areas and city centers. In

Fig. 3. Different population proportion (PP) of each region in Changsha main city. (a) Work-time (10 am) Active PP according to heatmap. (b) Rest-time (10 pm) Active PP according to heatmap. (c) The relative difference between (a) and (b). (d) Census PP according to WorldPop.

addition, we define the highly underestimated or overestimated PWE of the regions where the absolute value of the hourly difference between the active PWE and census PWE is greater than 2. Among them, the exposure at No. 68 Ansha Town (rural area) is overrated much, with the difference lower than -5 μg/m^3 during all time. On weekdays, most highly underestimated PWE is concentrated in suburban transportation hub like District 67 and industrial hub like District 73, with the daily average difference of 2 μg/m^3, 1 μg/m^3, respectively. While on weekends, in addition to the above two regions, the highly underestimated PWE appear in scenic areas such as District 26 and mixed-use zones such as District 52, with the daily average difference of 2 μg/m^3, 3 μg/m^3, respectively. Specific differences of PWE between two scenarios in individual regions are shown in Figs. S4–S5.

It is interesting that comparing exposure results in the same area can be opposite during morning and night, weekdays and weekends. For instance, in Orange island (No.26), the difference value at weekday night is lower than -2 μg/m^3 (largely overestimated), then it can come to more than 3 μg/m^3 (largely underestimated) on weekends. Opposite cases are in the airport zone (No.67), the difference is more than 2 μg/m^3 (largely underestimated) on weekdays while that is lower than -3 μg/m^3 (largely overestimated) at weekend night. The distributions of opposite-value regions change with the moving crowd at different times. Normally the exposure is more underestimated in people gathering areas.

3.2.3. Relative difference in PWE throughout the day

Fig. 5 shows the difference of $PM_{2.5}$ exposure in two scenarios in various regions of Changsha City throughout the day. It can be clearly observed that on both weekdays and weekends, the exposure in the sub-urban central area is underestimated a lot, while the exposure in the traditional city center (the eastern district) is often overestimated, especially on weekends. If the active PWE of the district is higher than census PWE for more than 12 h (from 7:00 to 23:00), we define the district is mainly underestimated. And if the active PWE of the district is lower than census PWE for more than 12 h (from 7:00 to 23:00), we define the district is mainly overestimated.

In no less than 12 time points on both study periods, 45.83% of suburbs' population-weighted exposure (PWE) is underestimated, while 100% of rural PWE and more than 34.78% of downtown's PWE is overestimated. In terms of the spatial distribution, the areas with more underestimated PWE are mainly concentrated in the transportation hubs (for example, Huanghua Airport in District 67, South Railway Station in District 60), and suburban industrial districts (like District 73 and its surrounding regions) on weekdays. On weekends, the PWE in the western inner city turns to be underestimated which is overestimated on weekdays.

3.2.4. Relative difference in PWE during different time periods

It is worth noting that distribution of areas with underestimated exposure on weekdays change significantly in each time period. We define the rush hours as 7:00–9:00, 17:00–19:00, a total of 6 time points on weekdays, and 8:00–9:00, 17:00–20:00, also 6 time points on weekends. The daytime is 10:00–11:00, 14:00–16:00, a total of 5 time points on weekdays, while 7 time points of 10:00–16:00 on weekends. The night rest is 21:00–23:00, 3 time points on both two days. The positive values (activity > census, underestimated) and negative values (activity < census, overestimated) which are determined in no less than 4 time points at peak time, no less than 4 time points during daytime on weekdays, no less than 5 time points during daytime on weekends, equal to 3 time points during the night rest periods are extracted, as shown in Fig. 6. The upper small diagram frames express the difference between the proportion of the population in the two scenarios.

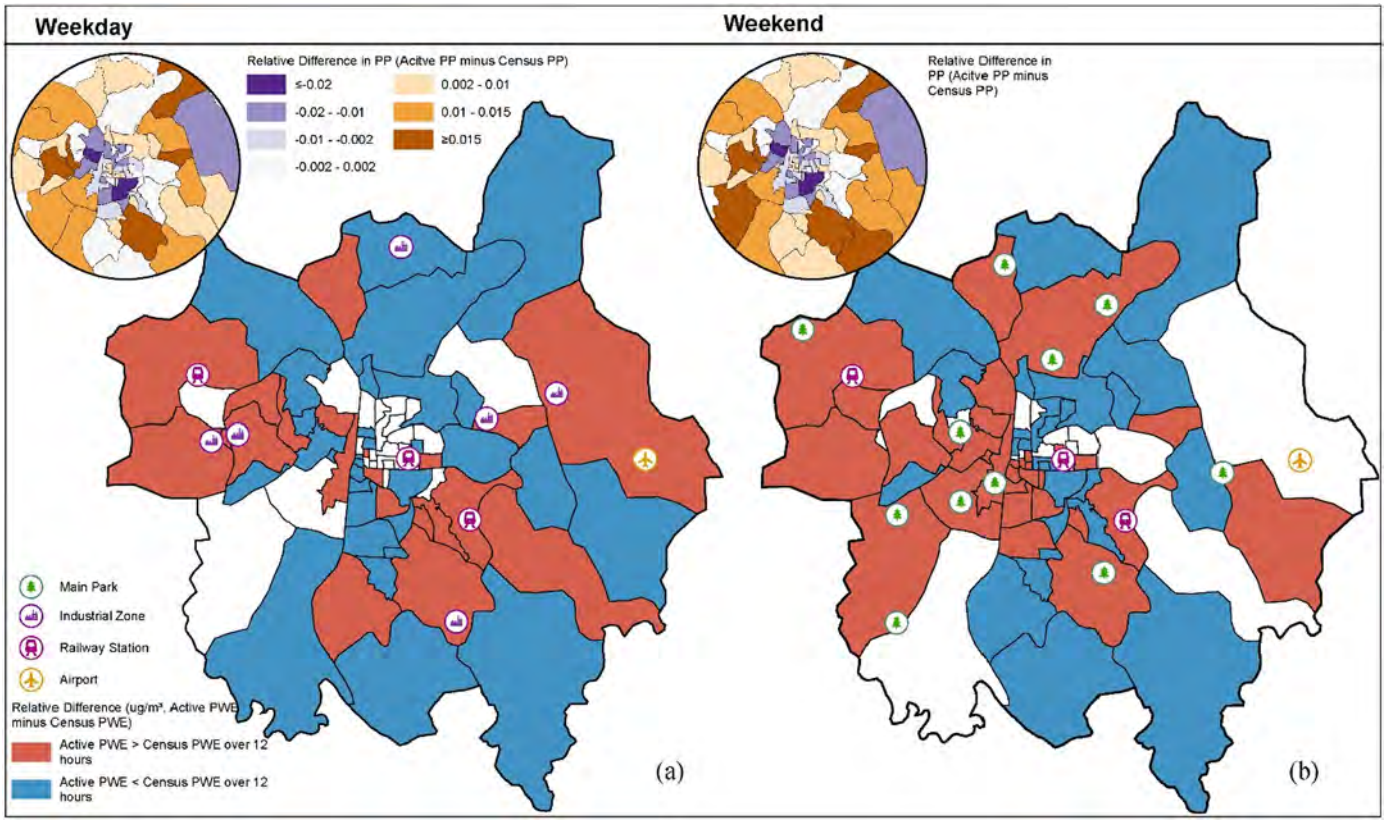

Fig. 5. The relative difference (μg/m^3) of PWE to $PM_{2.5}$ (μg/m^3) between active population scenario and census population scenario throughout the day, the red zone represents that active PWE is greater than census PWE in no less than 12 from 17 h, while the opposite is blue. (a) Is on weekday, (b) is on weekend. (Top-left of each frame) The difference between the proportions of the population using two computing methods. (For interpretation of the references to color in this figure legend, the reader is referred to the web version of this article.)

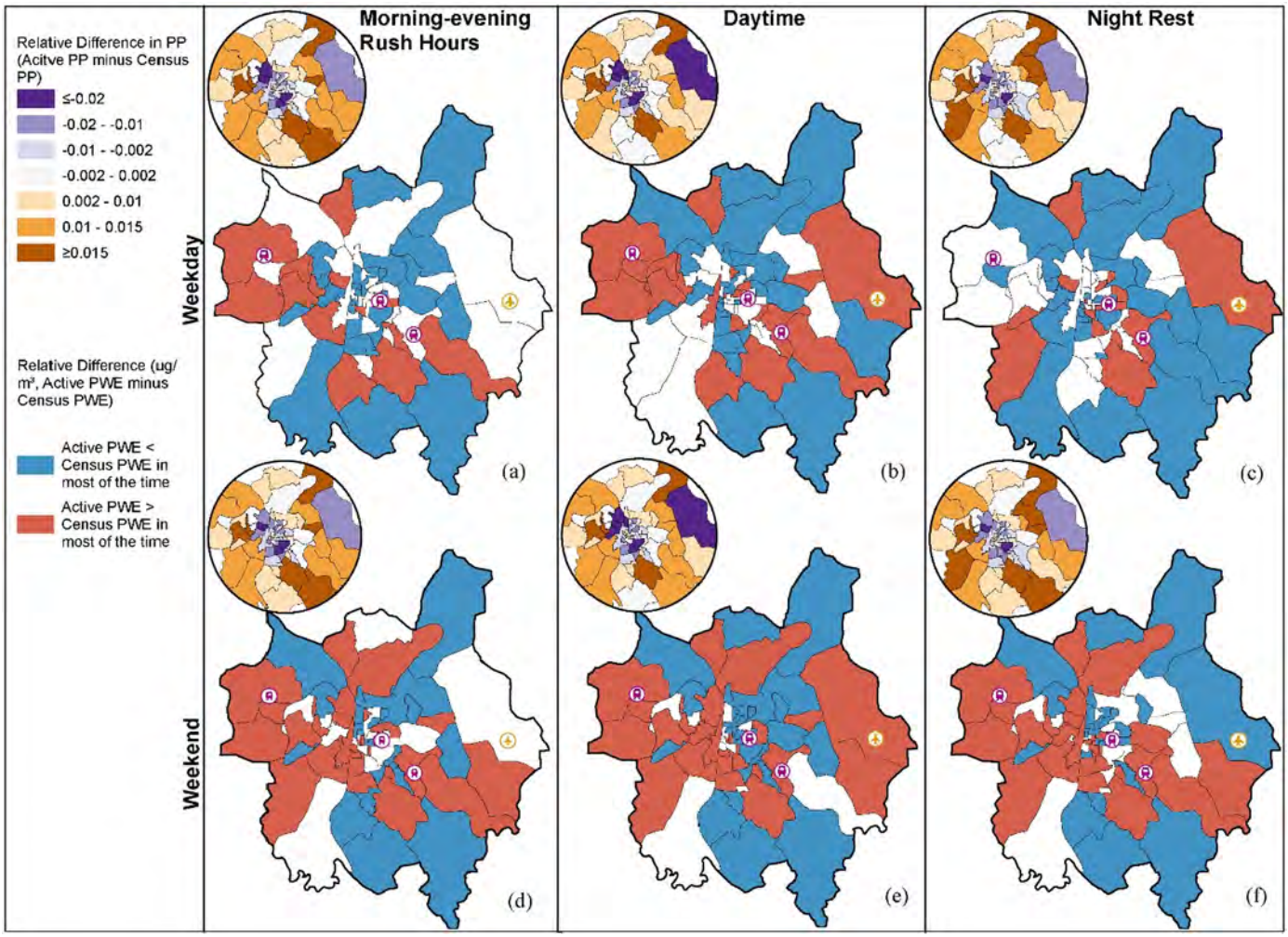

Fig. 6. The relative difference of PWE to $PM_{2.5}$ (μg/m^3) between active population scenario and census population scenario during different time periods. (a) (d) The difference in rush hours. (b) (e) The difference in day time. (c) (f) The difference in night-rest time. Top-left of each frame is the difference between the proportion of the population in two scenarios.

Specifically, on weekdays the underestimated areas are concentrated in the western and southern sub-urban areas in rush hours, with relatively high population proportion. Then the range is extended with the number of positive value regions increasing from 14 to 20 in the daytime, with the additions mainly distributed in downtown and the airport zones. At night the number of regions with positive value decreases from 20 to 16, and the regions are mostly concentrated in the eastern central city. It is interesting that the changes of the underestimated areas match up with the commuting trends. During weekends, the number of underestimated regions obviously grows, exceeding 30 on average. Compared to weekdays, the underestimated areas expand to western areas where most scenic spots are located, which is in accord with local people's movement on weekends during spring.

3.3. Relative difference in PWE in different regions

The results once again indicate the suburban exposure to $PM_{2.5}$ is more serious than expected; however, the downtown situation is less serious than previously thought. We select four representative locations from all 73 street-level communities, namely District 15 Pozi Street (traditional business district), District 37 Hanpu Town (sub-urban area), District 40 Dongfeng Road (city center of working and living function), District 60 Lituo Town (South Railway Station as the transport hub). Fig. 7 depicts the exposure of population active and census population from 7:00 to 23:00 on weekdays and weekends in these four locations. There is not much difference of the PWE in the two scenarios in the 15th district in the two days. While the active population exposure is greater in the 37th and 60th region (both are sub-urban areas) in the two days. In 40th Dongfeng Road, the exposure is less differentiating during weekdays and is overestimated more than 2 μg/m^3 throughout the weekends.

3.4. The total hourly PWE in Changsha City

To better present the hourly variation in $PM_{2.5}$ exposure, we aggregated the pixel-based assessments to obtain the hourly cumulative percentage of $PM_{2.5}$ exposure in the whole Changsha City. Fig. 8 illustrates the cumulative percentage of population and air pollution exposure determined for the two-calculation scenario. In both scenarios, almost 100% of the population in prime Changsha is exposed to $PM_{2.5}$ far exceeding the WHO limit of 25 μg/m^3. The $PM_{2.5}$ pollution is more serious on morning rush hours when half the urban population is exposed to more than 50 μg/m^3 and 70 μg/m^3 on weekdays and weekends, respectively. It is worth noting that the exposure to high-level $PM_{2.5}$ is greatly underestimated during the morning rush hours on weekdays. About 12.41% of urban people are exposed to $PM_{2.5}$ over 60 μg/m^3 in active scenario; meanwhile, the corresponding rate is only 5.92% for census population, leading to worse situation of $PM_{2.5}$ exposure for the commuters. In addition to the burden of long-distance commutes, they

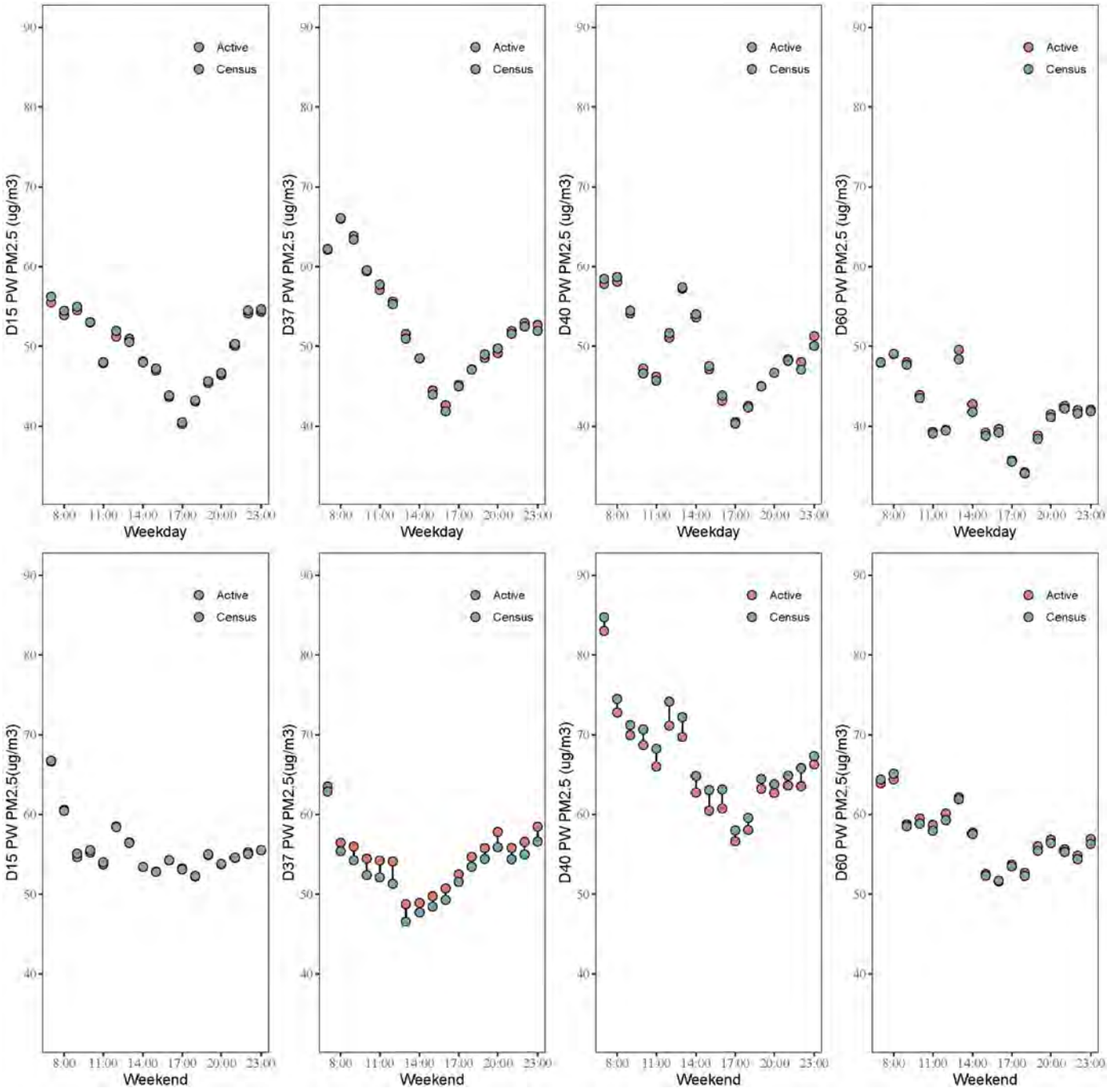

Fig. 7. PWE of active population and census population from 7:00 to 23:00 on weekdays and weekends in four typical locations.

have to run the risk of more health issues relative to air pollution. At other times, most of the active population's exposure is slightly lower.

4. Discussion

We take advantage of heatmap's characteristics of real time, large and diverse user base to build a dynamic population sample database which represents millions of people in Changsha City. The LBS big data of heatmap are used to define the changing distribution of the active population relative to the static rasterized census population. Then we analyze and compare the two types of PWE in 73 different street-level communities of Changsha City during different periods. In terms of spatial distribution of PWE, it is clearly observed that areas of high exposure value are mainly concentrated in traditional downtowns as people spend more time on work and leisure in these busy areas. However, through the comparative analysis, the downtown's PWE is often overestimated, while the underrated PWE is mainly in suburbs, especially on weekends. More notably, highly underestimated areas are also mainly concentrated in suburbs such as transportation hubs and new development zones. As for temporal distribution, it is interesting that comparing exposure results in the same area can be opposite during morning and night, weekdays and weekends, in accord with local people's movement. In addition, the exposure to high-level $PM_{2.5}$ is greatly underestimated during the morning rush hours on weekdays. About 12.41% of urban people are exposed to $PM_{2.5}$ over 60 μg/m^3,

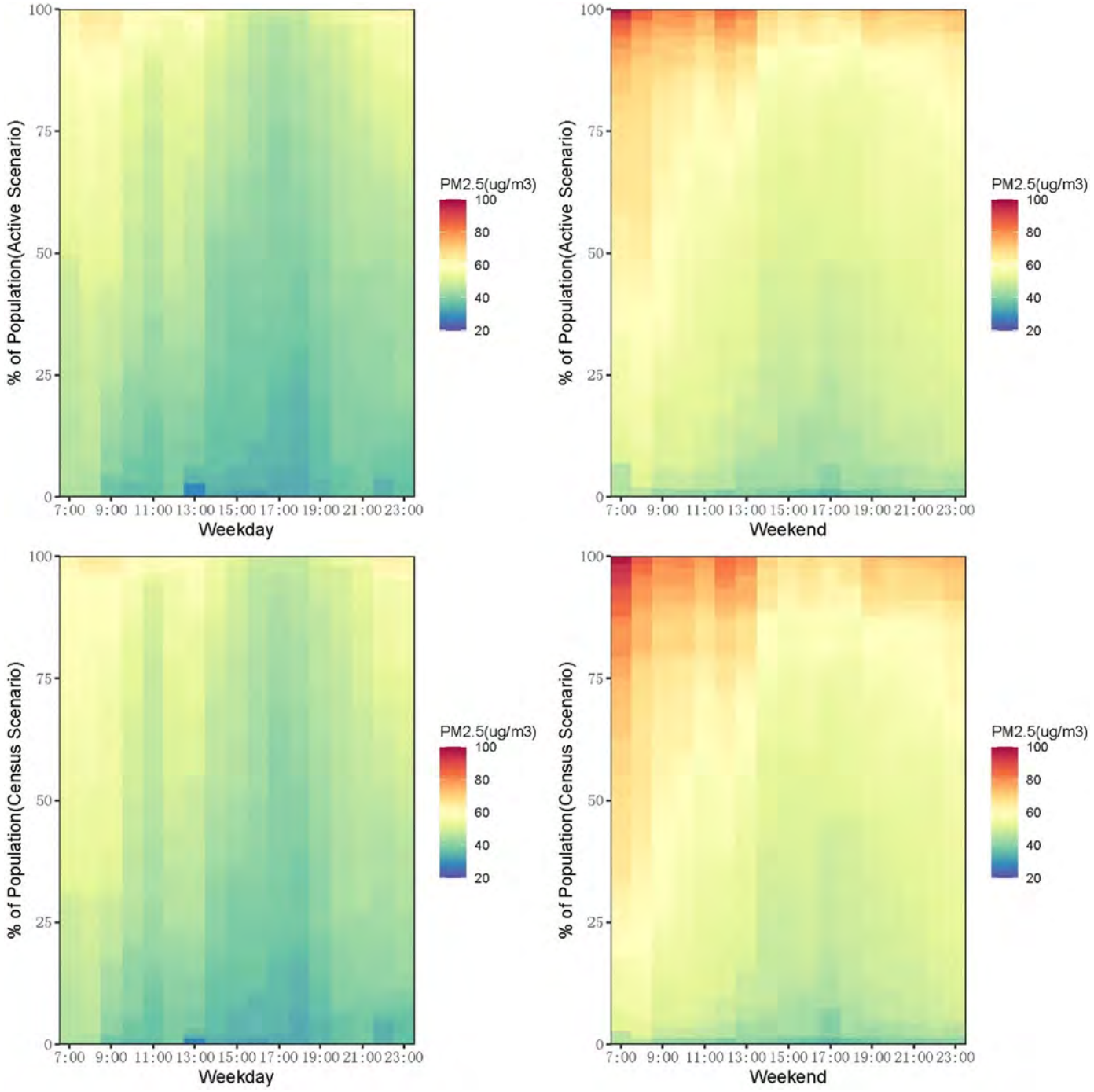

Fig. 8. Cumulative percentage of population and $PM_{2.5}$ exposure determined in two computing scenarios for each hour of weekdays and weekends.

about twice as much as that in census scenario, leading to worse situation of $PM_{2.5}$ exposure for the commuters.

Regarding the issue above, more attention should be paid to suburbs in Chinese metropolis with high-level $PM_{2.5}$ pollution, where the active crowds are massing no less than in city centers, and we can see the clear trend of outflow of urban people during rest periods and weekends. This phenomenon of short-term population mobility is a result of Chinese suburbanization process. Suburbanization in China began in the 1980s and has spread rapidly in large and medium-sized cities (Feng et al., 2009; Shen and Wu, 2013; Zhou and Ma, 2000). Most of China's suburban residents are purchasers of suburban commercial housing with far lower prices than that in the central city. These people mostly work in the city center and live in the suburbs, suffering from the long commutes and inequality in environmental resources (Day and Cervero, 2010; Hu et al., 2018; Li and Siu, 2010), such as the serious effects of exposure to $PM_{2.5}$ (Zhao, 2010). These unfair environmental resource distributions are attributable to unbalanced regional development which can also cause the spatio-temporal variability of air pollution. The results of the study can be applied to other regions of the world. Unlike the western developed countries, the developing countries such as Brazil and Colombia and some Asian developed countries like Japan have a fast suburbanization accompanied with rapidly expanding urbanization. Especially in the developing countries, people living in the cities of these countries usually experience a long commute by

taking public transit (Moovit, 2020), and are exposed to bad air during daily trips. Accurately estimating these commuters' exposure to air pollution especially in open environment, e.g., the walking route before and after taking public transit or driving is particularly important. We will narrow the research and focus on these target population in the further study.

By using varying spatiotemporal population metrics, studies can help to pinpoint the changing hotspots of high air pollution exposure. For example, as in this study, the different regions with bad air condition for commuters on weekdays in Changsha are found. Managers can take measures to improve the commuting environment according to actual situation. What is more, the application of micro-air monitoring stations and LBS big data is particularly suitable for dealing with short-term air pollution emergencies. They can accurately assess the dynamic population exposure in real time and help observers to find the location where the population exposure exceeds the limit in time. Therefore, the relative institutions can take steps quickly to avert an even worse situation.

The results of this study can be applied to optimize resource allocation, adjust the orientation of urban planning, thereby maximizing public health and related social and economic benefits. In the past, resources are too much inclined to traditional urban centers, ignoring suburbs. This research provides accurate and high-resolution data of population exposure to air pollution to help city managers make adjustments in urban planning and set down interventions to air pollution (e.g., setup of infrastructures, promote multi-functional complex of urban land use and balance the job-residence relation of the city). For instance, the infrastructures like monitoring stations can be established in areas with high population-weighted exposure to air pollutions, not only in downtown, but also the suburban regions. There is evidence that the correct adjustment of urban planning and appropriate interventions to air pollution can help reduce urban air pollution and improve people's health, such as lowering the morbidity of cardiovascular and respiratory diseases and the rate of premature deaths (Henschel et al., 2012; Pascal et al., 2013; Xu et al., 2020). In addition, air pollution is found to exert a significant impact on both public and national healthcare expenditure, as well as to drive the inequality in health care expenditure (Alimi et al., 2020; Liang et al., 2020; Sheng and Zhang, 2019; Yang and Zhang, 2018). Proper allocation of public spending also helps to cut down this part of expenditure.

There are some limitations in using the data of population mobility, however. First, LBS data is normally considered as non-representative data (Kwan, 2016; Song et al., 2019), the heatmap data used in the research actually represents the relative distribution of active users, not the true population density. The characteristics of big data of this type may not be fully sampled in some groups of population, such as children and the elderly. Nevertheless, the proportion of these groups of people using mobile networks is increasing significantly (China Internet Network Information Center, 2019), the sampling data bias of the minority groups will not weaken much the performance of LBS big data in characterizing distribution of dynamic population. Whereas, there are still some uncertainties when using such datasets, and these conclusions need to be treated with caution. Field surveys and interview questionnaires can be added for further verification in follow-up studies. Second, because the floating population between cities in a short period of time will not greatly affect the total population in the city, this study ignores the cross-city population flow and migration outside the urban area. Third, due to privacy and security concerns, LBS data cannot track individual path which makes it hard for us to distinguish the levels of population exposure to air pollution affected by different transportation options or commuting modes. This research focuses on the total amount of the large sample population; we can study the exposure of different groups of population by adding data of individuals in the future studies. Fourth, due to the limitations of Baidu heatmap API service, we can only get five days' data per city at most. Actually, each piece of heatmap has hundreds of thousands of data of a large sample size of population and the urban people's movements have regular daily and weekly patterns at urban scale. And then we analyzed the April's hourly $PM_{2.5}$ concentrations and found the laws that the $PM_{2.5}$ pollution was mainly worse at night and during the weekends in that April. Next, we may study people's exposure to air pollution in a larger range of time and space by applying for long-term and different cities' heatmap data.

This study proposes a new approach of calculating population exposure. We utilize two dynamic variables, namely micro-monitoring $PM_{2.5}$ data and heatmap population information to quantify the $PM_{2.5}$ exposure of active flow of millions of people in a highly urbanized metropolis. This study can offer a new idea to the field of environmental exposure science and environmental epidemiology and build a dataset for future research by combining the air quality with human health, which can also be extended to quantify other environmental issues and related health burdens. The findings of this study will help researchers and policy makers better understand the spatial pattern of air pollution and the impact of pollution exposure, thereby take effective measures to control pollution.

CRediT authorship contribution statement

Xin Li: Conceptualization, Methodology, Software, Data curation, Writing – original draft. **Tao Yang:** Validation, Supervision, Writing – review & editing. **Zhuotong Zeng:** Writing – review & editing. **Xiaodong Li:** Conceptualization, Supervision, Writing – review & editing. **Guangming Zeng:** Supervision, Writing – review & editing. **Jie Liang:** Conceptualization, Supervision, Writing – review & editing. **Rong Xiao:** Writing – review & editing. **Xuwu Chen:** Writing – review & editing.

Declaration of competing interest

The authors declare that they have no known competing financial interests or personal relationships that could have appeared to influence the work reported in this paper.

Acknowledgment

This work was supported by the Hunan Science & Technology Innovation Program (2018RS3037), the National Natural Science Foundation of China (51708192, 51979101, 51679082, 51521006, 82003363, 82073449, U20A20323, 52078196), the Natural Science Foundation of Hunan Province (2019JJ20002).

Appendix A. Supplementary data

Supplementary data to this article can be found online at https://doi.org/10.1016/j.scitotenv.2021.146283.

References

Alimi, O.Y., Ajide, K.B., Isola, W.A., 2020. Environmental quality and health expenditure in ECOWAS. Environ. Dev. Sustain. 22, 5105–5127.
Apte, J.S., Marshall, J.D., Cohen, A.J., Brauer, M., 2015. Addressing global mortality from ambient PM2.5. Environ. Sci. Technol. 49, 8057–8066.
Araki, S., Shima, M., Yamamoto, K., 2018. Spatiotemporal land use random forest model for estimating metropolitan NO2 exposure in Japan. Sci. Total Environ. 634, 1269–1277.
Carnevale, C., Finzi, G., Pisoni, E., Singh, V., Volta, M., 2011. An integrated air quality forecast system for a metropolitan area. J. Environ. Monit. 13, 3437–3447.
Chan, C.K., Yao, X., 2008. Air pollution in mega cities in China. Atmos. Environ. 42, 1–42.
Chan, E.Y.Y., Goggins, W.B., Kim, J.J., Griffiths, S.M., 2012. A study of intracity variation of temperature-related mortality and socioeconomic status among the Chinese population in Hong Kong. J. Epidemiol. Community Health 66, 322–327.
Chen, B., Song, Y., Jiang, T., Chen, Z., Huang, B., Xu, B., 2018. Real-time estimation of population exposure to PM2.5 using mobile- and station-based big data. Int. J. Environ. Res. Public. Health 15, 573.
China Internet Network Information Center, 2019. The 44th China Statistical Report on Internet Development (in Chinese) [WWW Document]. URL http://www.cac.gov.cn/2019-08/30/c_1124938750.htm (accessed 9.20.20).
Cohen, A.J., Brauer, M., Burnett, R., Anderson, H.R., Frostad, J., Estep, K., Balakrishnan, K., Brunekreef, B., Dandona, L., Dandona, R., Feigin, V., Freedman, G., Hubbell, B.,

Jobling, A., Kan, H., Knibbs, L., Liu, Y., Martin, R., Morawska, L., Pope III, C.A., Shin, H., Straif, K., Shaddick, G., Thomas, M., van Dingenen, R., van Donkelaar, A., Vos, T., Murray, C.J.L., Forouzanfar, M.H., 2017. Estimates and 25-year trends of the global burden of disease attributable to ambient air pollution: an analysis of data from the Global Burden of Diseases Study 2015. Lancet 389, 1907–1918.

Day, J., Cervero, R., 2010. Effects of residential relocation on household and commuting expenditures in Shanghai. China. Int. J. Urban Reg. Res. 34, 762–788.

Dobson, J.E., Bright, E.A., Coleman, P.R., Durfee, R.C., Worley, B.A., 2000. LandScan: a global population database for estimating populations at risk. Photogramm. Eng. Remote. Sens. 66, 849–857.

Dominici, F., Peng, R.D., Bell, M.L., Pham, L., McDermott, A., Zeger, S.L., Samet, J.M., 2006. Fine particulate air pollution and hospital admission for cardiovascular and respiratory diseases. Jama-J. Am. Med. Assoc. 295, 1127–1134.

Feng, J., Wang, F., Zhou, Y., 2009. The spatial restructuring of population in metropolitan Beijing: toward polycentricity in the post-reform era. Urban Geogr. 30, 779–802.

Fleischer, N.L., Merialdi, M., van Donkelaar, A., Vadillo-Ortega, F., Martin, R.V., Betran, A.P., Souza, J.P., O'Neill, M.S., 2014. Outdoor air pollution, preterm birth, and low birth weight: analysis of the World Health Organization global survey on maternal and perinatal health. Environ. Health Perspect. 122, 425–430.

Gariazzo, C., Carlino, G., Silibello, C., Renzi, M., Finardi, S., Pepe, N., Radice, P., Forastiere, F., Michelozzi, P., Viegi, G., Stafoggia, M., 2020. A multi-city air pollution population exposure study: combined use of chemical-transport and random-Forest models with dynamic population data. Sci. Total Environ. 724, 138102.

Gui, K., Che, H., Wang, Y., Wang, H., Zhang, L., Zhao, H., Zheng, Y., Sun, T., Zhang, X., 2019. Satellite-derived PM2.5 concentration trends over Eastern China from 1998 to 2016: relationships to emissions and meteorological parameters. Environ. Pollut. 247, 1125–1133.

Hankey, S., Sforza, P., Pierson, M., 2019. Using mobile monitoring to develop hourly empirical models of particulate air pollution in a rural Appalachian community. Environ. Sci. Technol. 53, 4305–4315.

Hay, S.I., Noor, A.M., Nelson, A., Tatem, A.J., 2005. The accuracy of human population maps for public health application. Tropical Med. Int. Health 10, 1073–1086.

Henschel, S., Atkinson, R., Zeka, A., Le Tertre, A., Analitis, A., Katsouyanni, K., Chanel, O., Pascal, M., Forsberg, B., Medina, S., Goodman, P.G., 2012. Air pollution interventions and their impact on public health. Int. J. Public Health 57, 757–768.

Ho, H.C., Knudby, A., Huang, W., 2015. A spatial framework to map heat health risks at multiple scales. Int. J. Environ. Res. Public Health 12, 16110–16123.

Hoek, G., Krishnan, R.M., Beelen, R., Peters, A., Ostro, B., Brunekreef, B., Kaufman, J.D., 2013. Long-term air pollution exposure and cardio-respiratory mortality: a review. Environ. Health 12, 43.

Hu, L., Sun, T., Wang, L., 2018. Evolving urban spatial structure and commuting patterns: a case study of Beijing. China. Transp. Res. Part Transp. Environ. 59, 11–22.

Kampa, M., Castanas, E., 2008. Human health effects of air pollution. Environ. Pollut. 151, 362–367.

Kim, K.-H., Kabir, E., Kabir, S., 2015. A review on the human health impact of airborne particulate matter. Environ. Int. 74, 136–143.

Kwan, M.P., 2016. Algorithmic geographies: big data, algorithmic uncertainty, and the production of geographic knowledge. Ann. Am. Assoc. Geogr. 106, 274–282.

Laden, F., Neas, L.M., Dockery, D.W., Schwartz, J., 2000. Association of fine particulate matter from different sources with daily mortality in six U.S. cities. Environ. Health Perspect. 108, 941–947.

Lee, M., Brauer, M., Wong, P., Tang, R., Tsui, T.H., Choi, C., Cheng, W., Lai, P., Tian, L., Thach, T.-Q., Allen, R., Barratt, B., 2017. Land use regression modelling of air pollution in high density high rise cities: a case study in Hong Kong. Ence Total Environ. 595, 306–315.

Leng, B., Yu, Y., Huang, D., Yi, Z., 2015. Big data based job-residence relation in Chongqing metropolitan area (in Chinese). Planners 31, 92–96.

Li, S.M., Siu, Y.M., 2010. Residential mobility and urban restructuring under market transition: a study of Guangzhou. China. Prof. Geogr. 53, 219–229.

Li, H., Qian, X., Hu, W., Wang, Y., Gao, H., 2013. Chemical speciation and human health risk of trace metals in urban street dusts from a metropolitan city, Nanjing. SE China. Sci. Total Environ. 456–457, 212–221.

Li, X., Liu, W., Chen, Z., Zeng, G., Hu, C., León, T., Liang, J., Huang, G., Gao, Z., Li, Z., Yan, W., He, X., Lai, M., He, Y., 2015. The application of semicircular-buffer-based land use regression models incorporating wind direction in predicting quarterly NO2 and PM10 concentrations. Atmos. Environ. 103, 18–24.

Li, X., Chen, X., Yuan, Xingzhong, Zeng, G., León, T., Liang, J., Chen, G., Yuan, Xinliang, 2017. Characteristics of particulate pollution (PM2.5 and PM10) and their spacescale-dependent relationships with meteorological elements in China. Sustainability 9, 2330.

Li, R., Cui, L., Meng, Y., Zhao, Y., Fu, H., 2019. Satellite-based prediction of daily SO2 exposure across China using a high-quality random forest-spatiotemporal Kriging (RF-STK) model for health risk assessment. Atmos. Environ. 208, 10–19.

Liang, J., Liu, Q., Zhang, H., Li, Xiaodong, Qian, Z., Lei, M., Li, Xin, Peng, Y., Li, S., Zeng, G., 2020. Interactive effects of climate variability and human activities on blue and green water scarcity in rapidly developing watershed. J. Clean. Prod. 265, 121834.

Lin, C.Q., Liu, G., Lau, A.K.H., Li, Y., Li, C.C., Fung, J.C.H., Lao, X.Q., 2018. High-resolution satellite remote sensing of provincial PM2.5 trends in China from 2001 to 2015. Atmos. Environ. 180, 110–116.

Liu, X.G., Li, J., Qu, Y., Han, T., Hou, L., Gu, J., Chen, C., Yang, Y., Liu, X., Yang, T., Zhang, Y., Tian, H., Hu, M., 2013. Formation and evolution mechanism of regional haze: a case study in the megacity Beijing. China. Atmospheric Chem. Phys. 13, 4501–4514.

Liu, W., Li, X., Chen, Z., Zeng, G., León, T., Liang, J., Huang, G., Gao, Z., Jiao, S., He, X., Lai, M., 2015. Land use regression models coupled with meteorology to model spatial and temporal variability of NO2 and PM10 in Changsha. China. Atmos. Environ. 116, 272–280.

Lu, Y., Fang, T.B., 2015. Examining personal air pollution exposure, intake, and health danger zone using time geography and 3D geovisualization. ISPRS Int. J. Geo-Inf. 4, 32–46.

Lu, M., Sun, C., Zheng, S., 2017. Congestion and pollution consequences of driving-to-school trips: a case study in Beijing. Transp. Res. Part Transp. Environ. 50, 280–291.

Miller, K.A., Siscovick, D.S., Sheppard, L., Shepherd, K., Sullivan, J.H., Anderson, G.L., Kaufman, J.D., 2007. Long-term exposure to air pollution and incidence of cardiovascular events in women. N. Engl. J. Med. 356, 447–458.

Moovit, 2020. Global Public Transport Report 2020 [WWW Document]. URL https://moovitapp.com/insights/en/Moovit_Insights_Public_Transit_Index-countries (accessed 1.28.21).

Nethery, E., Leckie, S.E., Teschke, K., Brauer, M., 2008. From measures to models: an evaluation of air pollution exposure assessment for epidemiological studies of pregnant women. Occup. Environ. Med. 65, 579–586.

Nyhan, M., Grauwin, S., Britter, R., Misstear, B., McNabola, A., Laden, F., Barrett, S.R.H., Ratti, C., 2016. "Exposure track"—the impact of mobile-device-based mobility patterns on quantifying population exposure to air pollution. Environ. Sci. Technol. 50, 9671–9681.

Nyhan, M., Kloog, I., Britter, R., Ratti, C., Koutrakis, P., 2019. Quantifying population exposure to air pollution using individual mobility patterns inferred from mobile phone data. J. Expo. Sci. Environ. Epidemiol. 29.

Pascal, M., Corso, M., Chanel, O., Declercq, C., Badaloni, C., Cesaroni, G., Henschel, S., Meister, K., Haluza, D., Martin-Olmedo, P., Medina, S., 2013. Assessing the public health impacts of urban air pollution in 25 European cities: results of the Aphekom project. Sci. Total Environ. 449, 390–400.

Peters, A., Dockery, D.W., Muller, J.E., Mittleman, M.A., 2001. Increased particulate air pollution and the triggering of myocardial infarction. Circulation 103, 2810–2815.

Reed, F.J., Gaughan, A.E., Stevens, F.R., Yetman, G., Sorichetta, A., Tatem, A.J., 2018. Gridded population maps informed by different built settlement products. Data 3, 33.

Rijnders, E., Janssen, N.A.H., van Vliet, P.H.N., Brunekreef, B., 2001. Personal and outdoor nitrogen dioxide concentrations in relation to degree of urbanization and traffic density. Environ. Health Perspect. 109, 411–417.

Setton, E., Marshall, J.D., Brauer, M., Lundquist, K.R., Hystad, P., Keller, P., Cloutier-Fisher, D., 2011. The impact of daily mobility on exposure to traffic-related air pollution and health effect estimates. J. Expo. Sci. Environ. Epidemiol. 21, 42–48.

Shen, J., Wu, F., 2013. Moving to the suburbs: demand-side driving forces of suburban growth in China. Environ. Plan. A 45, 1823–1844.

Sheng, P., Zhang, Y., 2019. The effect of pollution on the inequality in health care expenditure: evidence from China. Energy Environ. 30, 1380–1395.

Singh, V., Carnevale, C., Finzi, G., Pisoni, E., Volta, M., 2011. A cokriging based approach to reconstruct air pollution maps, processing measurement station concentrations and deterministic model simulations. Environ. Model. Softw. 26, 778–786.

Song, Y., Huang, B., He, Q., Chen, B., Wei, J., Mahmood, R., 2019. Dynamic assessment of PM2.5 exposure and health risk using remote sensing and geo-spatial big data. Environ. Pollut. 253, 288–296.

Stafoggia, M., Bellander, T., Bucci, S., Davoli, M., de Hoogh, K., de' Donato, F., Gariazzo, C., Lyapustin, A., Michelozzi, P., Renzi, M., Scortichini, M., Shtein, A., Viegi, G., Kloog, I., Schwartz, J., 2019. Estimation of daily PM10 and PM2.5 concentrations in Italy, 2013–2015, using a spatiotemporal land-use random-forest model. Environ. Int. 124, 170–179.

Stevens, F.R., Gaughan, A.E., Linard, C., Tatem, A.J., 2015. Disaggregating census data for population mapping using random forests with remotely-sensed and ancillary data. PLoS One 10, e0107042.

Stevens, F.R., Gaughan, A.E., Nieves, J.J., King, A., Sorichetta, A., Linard, C., Tatem, A.J., 2020. Comparisons of two global built area land cover datasets in methods to disaggregate human population in eleven countries from the global South. Int. J. Digit. Earth 13, 78–100.

Tai, H., 2019. Research on the population space-time convergence in the five districts in Dalian City (in Chinese). Hous. Sci. 39, 23–27.

Tan, X., Huang, D., Zhao, X., Yu, Y., Leng, B., Feng, L., 2016. The measurement of job-residence balance based on Baidu Heatmap (in Chinese). J. Beijing Norm. Univ. Nat. Sci. 52, 622–627.

Tatem, A.J., Hay, S.I., 2004. Measuring urbanization pattern and extent for malaria research: a review of remote sensing approaches. J. Urban Health 81, 363–376.

Tatem, A.J., Noor, A.M., Hay, S.I., 2004. Defining approaches to settlement mapping for public health management in Kenya using medium spatial resolution satellite imagery. Remote Sens. Environ. 93, 42–52.

Tatem, A.J., Noor, A.M., Hay, S.I., 2005. Assessing the accuracy of satellite derived global and national urban maps in Kenya. Remote Sens. Environ. 96, 87–97.

Wang, L., 2018. Spatial-temporal characteristics of urban population aggregation based on Baidu heat map in central areas of Wuhan City (in Chinese). J. Hum. Settl. West China 2, 52–56.

Wu, Z., Ye, Z., 2016. Research on urban spatial structure based on heatmap: a case study on the central city of Shanghai (in Chinese). City Plan. Rev. 347, 33–40.

Wu, J., Winer, A.M., Delfino, R.J., 2006. Exposure assessment of particulate matter air pollution before, during, and after the 2003 Southern California wildfires. Atmos. Environ. 40, 3333–3348.

Xu, M., Sbihi, H., Pan, X., Brauer, M., 2019. Local variation of PM2.5 and NO2 concentrations within metropolitan Beijing. Atmos. Environ. 200, 254–263.

Xu, W., Zeng, Z., Xu, Z., Li, Xiaodong, Chen, X., Li, Xin, Xiao, R., Liang, J., Chen, G., Lin, A., Li, J., Zeng, G., 2020. Public health benefits of optimizing urban industrial land layout - the case of Changsha. China. Environ. Pollut. 263, 114388.

Yang, J., Zhang, B., 2018. Air pollution and healthcare expenditure: implication for the benefit of air pollution control in China. Environ. Int. 120, 443–455.

Zhang, Q., Crooks, R., 2012. Toward an environmentally sustainable future: country environmental analysis of the People's Republic of China (Asian Development Bank).

Zhang, H., Wang, Z., Zhang, W., 2016. Exploring spatiotemporal patterns of PM2.5 in China based on ground-level observations for 190 cities. Environ. Pollut. 216, 559–567.
Zhao, P., 2010. Sustainable urban expansion and transportation in a growing megacity: consequences of urban sprawl for mobility on the urban fringe of Beijing. Habitat Int. 34, 236–243.
Zhao, X., Cheng, H., He, S., Cui, X., Pu, X., Lu, L., 2018. Spatial associations between social groups and ozone air pollution exposure in the Beijing urban area. Environ. Res. 164, 173–183.
Zhou, Y.X., Ma, L.J.C., 2000. Economic restructuring and suburbanization in China. Urban Geogr. 21, 205–236.